B.3 TEST RESULTS

In this section experimental results are presented and discussed. Particular attention is given to the influence of axle load, vehicle speed and accumulating traffic on the behaviour of the vehicle/track system.

B.3.1 Influence of Axle Load on Track Behaviour

The influence of axle load on track behaviour, in particular the effect on the dynamic track stiffness and the ratio between the sleeper reaction and the wheel load was investigated. Figure B29 shows the sleeper deflection, the sleeper reaction, the wheel load, and Figure B30 the resultant dynamic track stiffness as the long test train travelled over a particular sleeper in the test section. It was found that, as the wheel load increased, the ratio of the sleeper reaction force to the applied wheel load increased. This is due to the fact that the length of the deflection basin does not increase significantly with an increase in vertical loading. The increase in the sleeper deflection, and the sleeper reaction to wheel load ratio, as a function of increasing wheel load is shown in Figure B31.

A closer examination of Figure B30 shows that there is no significant difference in the path of the dynamic downward stroke due to changes in the wheel load. The only difference is that the amount of track deflection increases with increasing wheel load. Also seen in Figure B30 is the increase in structural damping due to increased wheel loading.

Another observation in the graph of the dynamic track stiffness can be seen in the grey shaded area. This area represents the dynamic track behaviour due to the wheels in the trailing bogie of one CCL-5 wagon and the wheels of the leading bogie of the next CCL-5 wagon. Due to the short axle spacing the track is not able to return to zero deflection and thus a significant change in sleeper reaction occurs with only a small change in sleeper deflection. Very little damping is observed

under these conditions. When long wheel base rail vehicles like locomotives move over the track the situation is different and the track is able to return to zero deflection between the wheelsets. This can be seen in Figure B26.

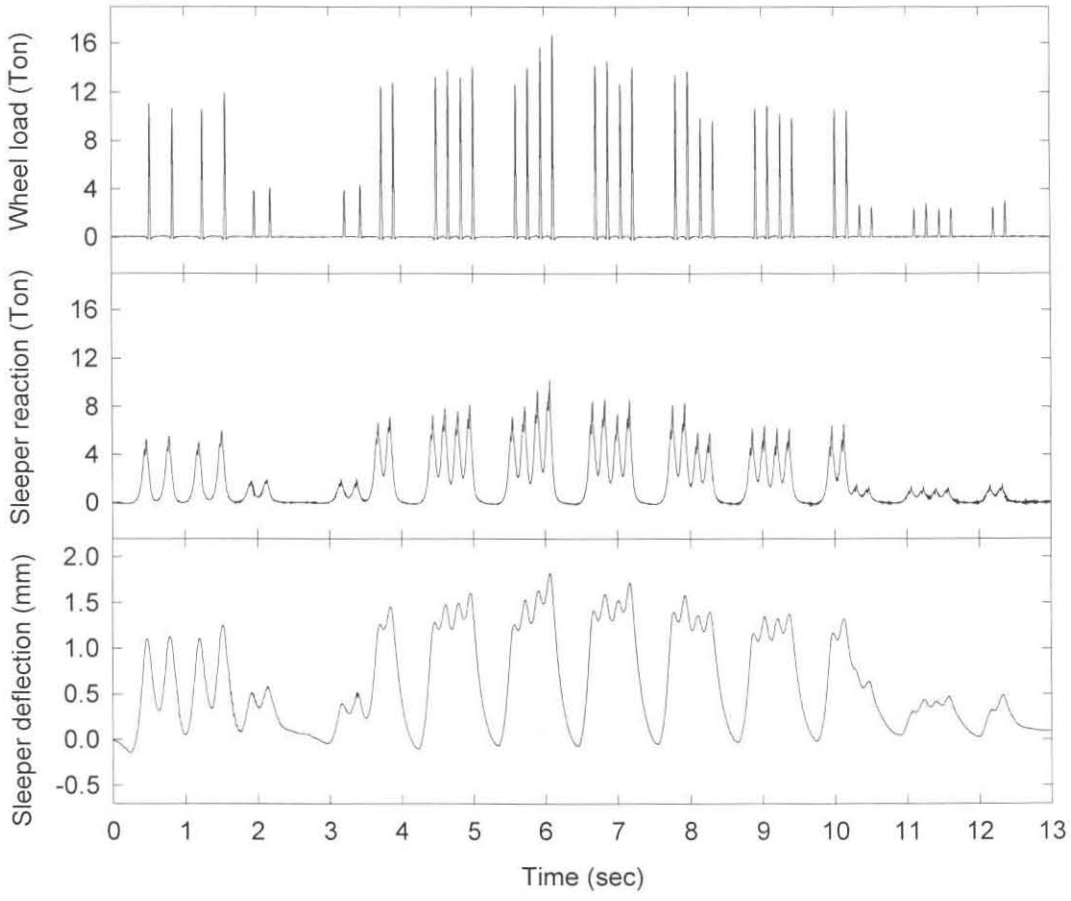

Figure B29: Dynamic track behaviour under varying wheel loads.

B.3.2 Vehicle and Track Performance as a Function of Vehicle Speed

In this section the influence of vehicle speed on the dynamic wheel load, the dynamic performance of the secondary suspension of the vehicle and the dynamic behaviour of the track is presented.

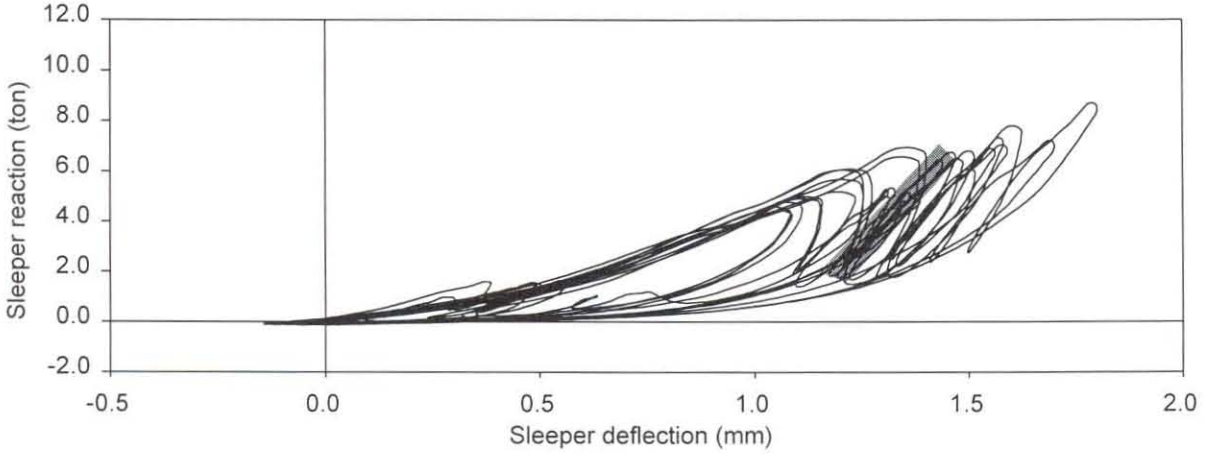

Figure B30: Dynamic track stiffness under varying wheel loads.

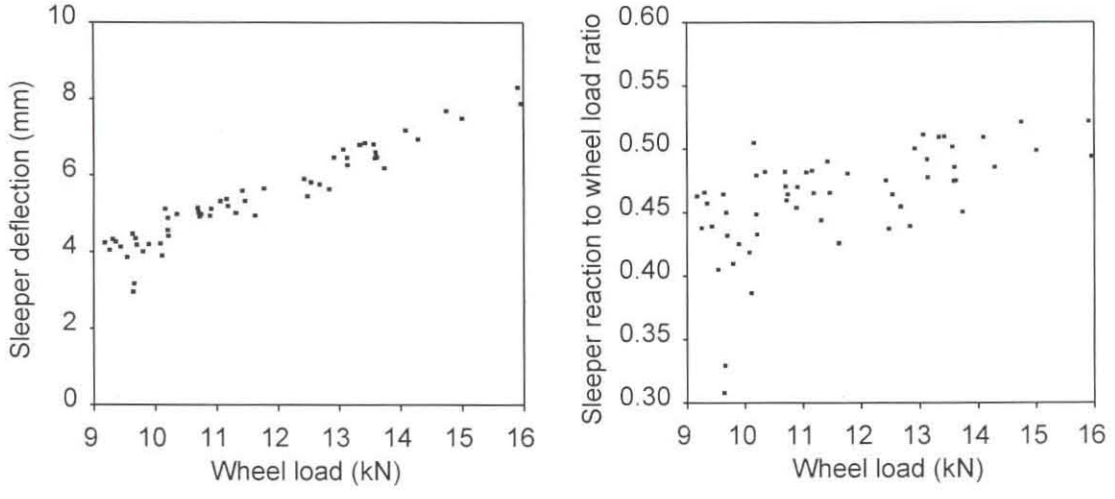

Figure B31: Influence of vehicle load on track behaviour.

B.3.2.1 Dynamic Wheel Load

In Figure B32 the dynamic wheel load as measured by the left wheel of the load measuring wheelset is shown for various vehicle speeds and in Figure B33 the Root Mean Square (RMS) values of the dynamic wheel load are plotted against vehicle speed at various stages of accumulating traffic. From these graphs it can be seen that by reducing the speed of trains passing over a deteriorated track, the dynamic wheel load can be reduced. The increase in the dynamic wheel load with accumulating traffic is due to the increase in track roughness with accumulating traffic.

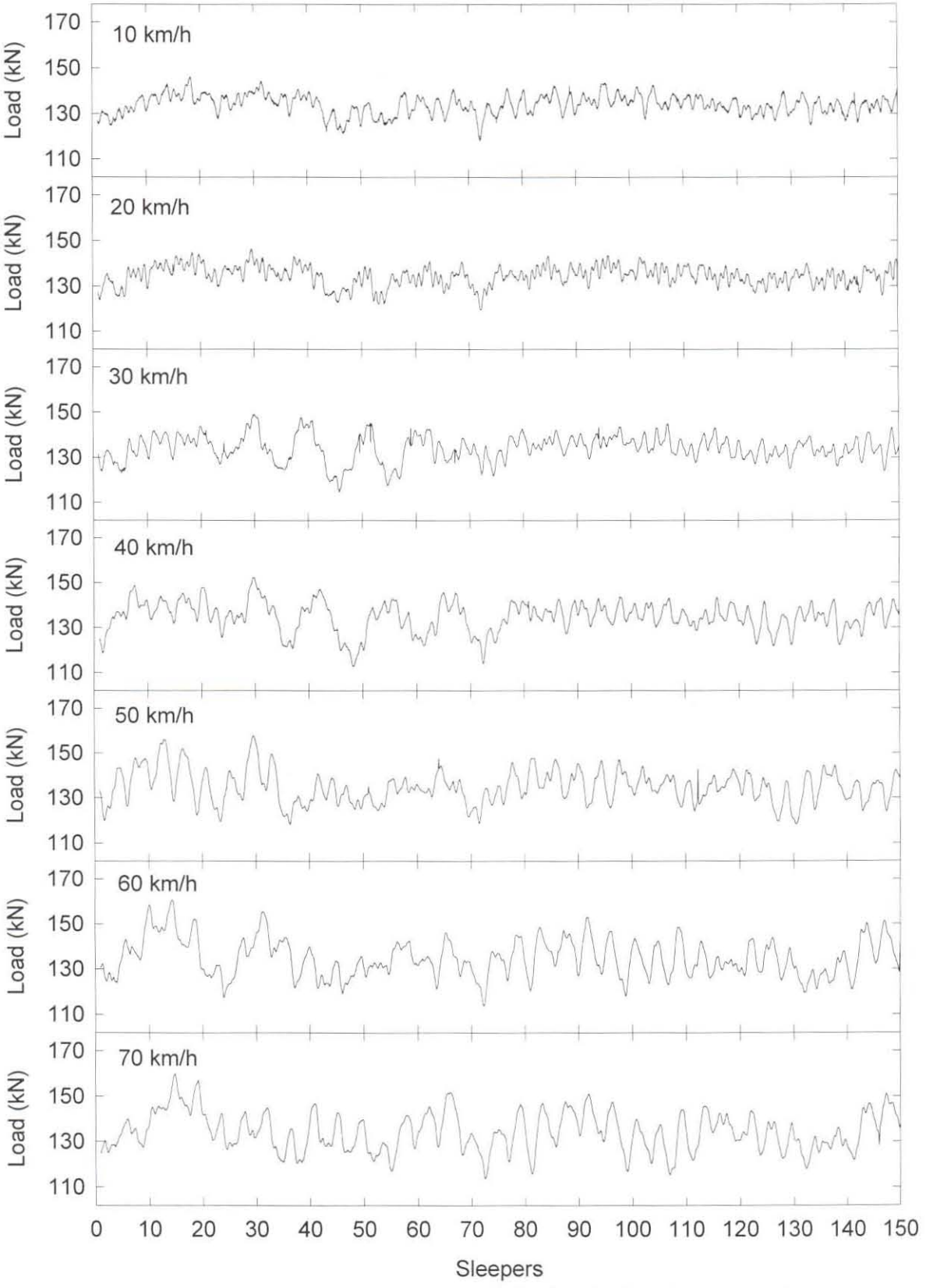

Figure B32: Dynamic wheel loads under the left wheel at various speeds.

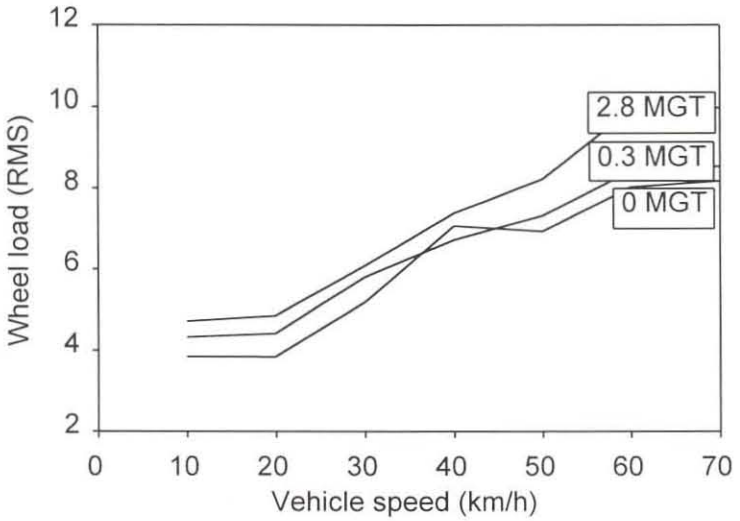

Figure B33: Dynamic wheel load as a function of vehicle speed.

In Figure B34 the Power Spectral Density (PSD) values for the body roll and bounce frequencies as measured in terms of the wheel load are shown for vehicle speeds ranging from 10km/h to 70km/h. The PSD provides information about the statistical properties of the signal in the frequency domain by showing how the energy of the signal is distributed over the frequency range.

The PSD values were calculated using the Fast Fourier Transform (FFT) algorithm (Bendat and Piersol, 1971). When calculating the PSD, frequency smoothing was applied. This means that the average value of the PSD was calculated at a certain frequency in a narrow bandwidth. For the PSD graphs shown in Figure B34 a normalized standard error of 0.5 was used. The definition of the normalized standard error is given by:

$$\epsilon_r = \sqrt{1/l_{fc}} \tag{B4}$$

where l_{fc} is the number of neighbouring frequency components. The effective resolution bandwidth is defined as:

$$B_e' = l_{fc}/T = \frac{1}{\epsilon_r^2\ T} \tag{B5}$$

where T is the total measuring time. For example if T is 33.31 seconds and the normalized standard error is 0.5, the effective resolution bandwidth is 0.1201 Hz. Calculations of the PSD values were done using the program RDAP (Fröhling, 1994). From the graphs in Figure B34 it is clear that the frequency pattern changes with increasing vehicle speed. These changes are due to the occurrence of resonance in the suspension system at certain vehicle speeds, out-of-round wheels, and track geometry input excitations.

B.3.2.2 Vehicle Performance

The performance of the test vehicle is given in terms of the vertical displacement across the secondary suspension of the bogie. Time traces of the vertical displacement across the secondary suspension for vehicle speeds from 10km/h to 70km/h are shown in Figure B35. As can be seen, the displacement shows a tendency to increase with increasing vehicle speed. However, due to the non-linearity in the secondary suspension system, the displacement is often abrupt and unpredictable. Due to the relatively good condition of the track, the displacement in the secondary suspension is also very small, reaching a maximum displacement of only approximately 3mm.

B.3.2.3 Dynamic Track Behaviour

The dynamic behaviour of the track as a function of vehicle speed is discussed in terms of sleeper deflection, sleeper reaction, wheel load, and the ratio between the sleeper reaction and the wheel load. Figure B36 shows a 8% decrease in the sleeper deflection with increasing vehicle speed. In absolute terms the decrease is only 0.1mm. Figure B36 also shows a small increase in the sleeper reaction, the dynamic wheel load and the sleeper reaction to wheel load ratio with increasing vehicle speed. At around 30km/h there are a few stray points due to nonlinearities in the vehicle suspension system and the natural frequencies of the vehicle components as well as wave lengths of track input.

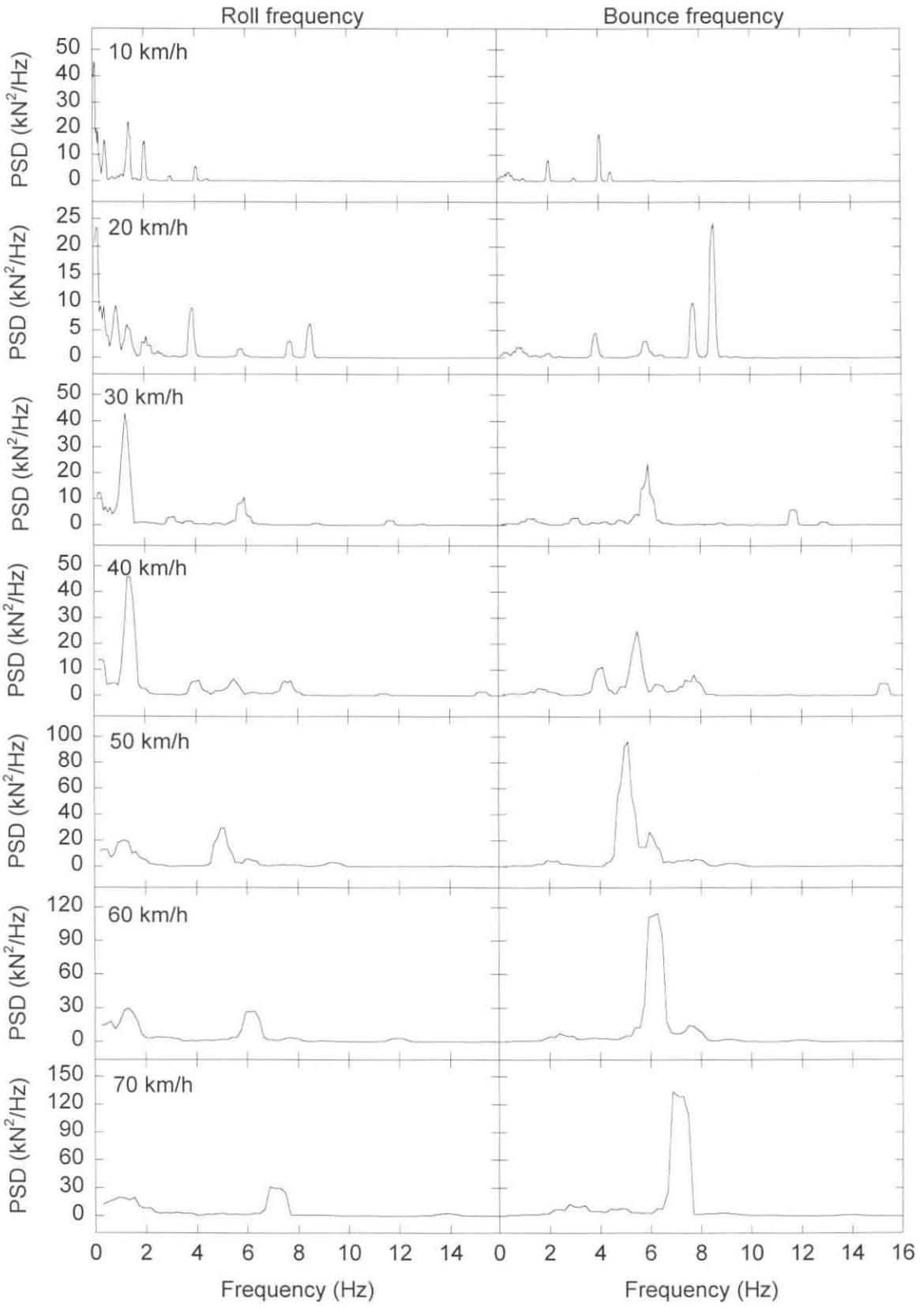

Figure B34: Frequency response as a function of vehicle speed.

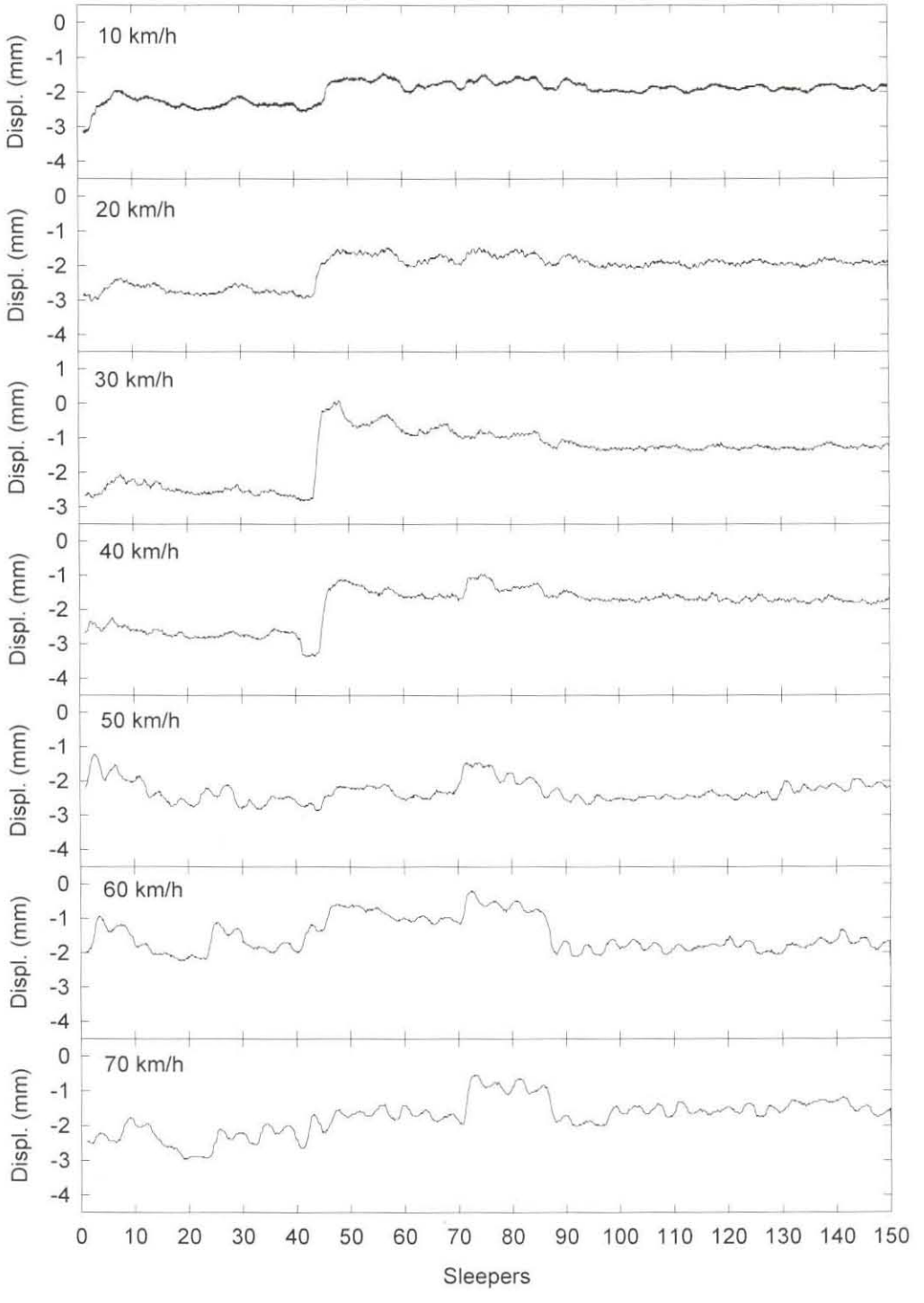

Figure B35: Vertical displacement across secondary suspension as a function of vehicle speed.

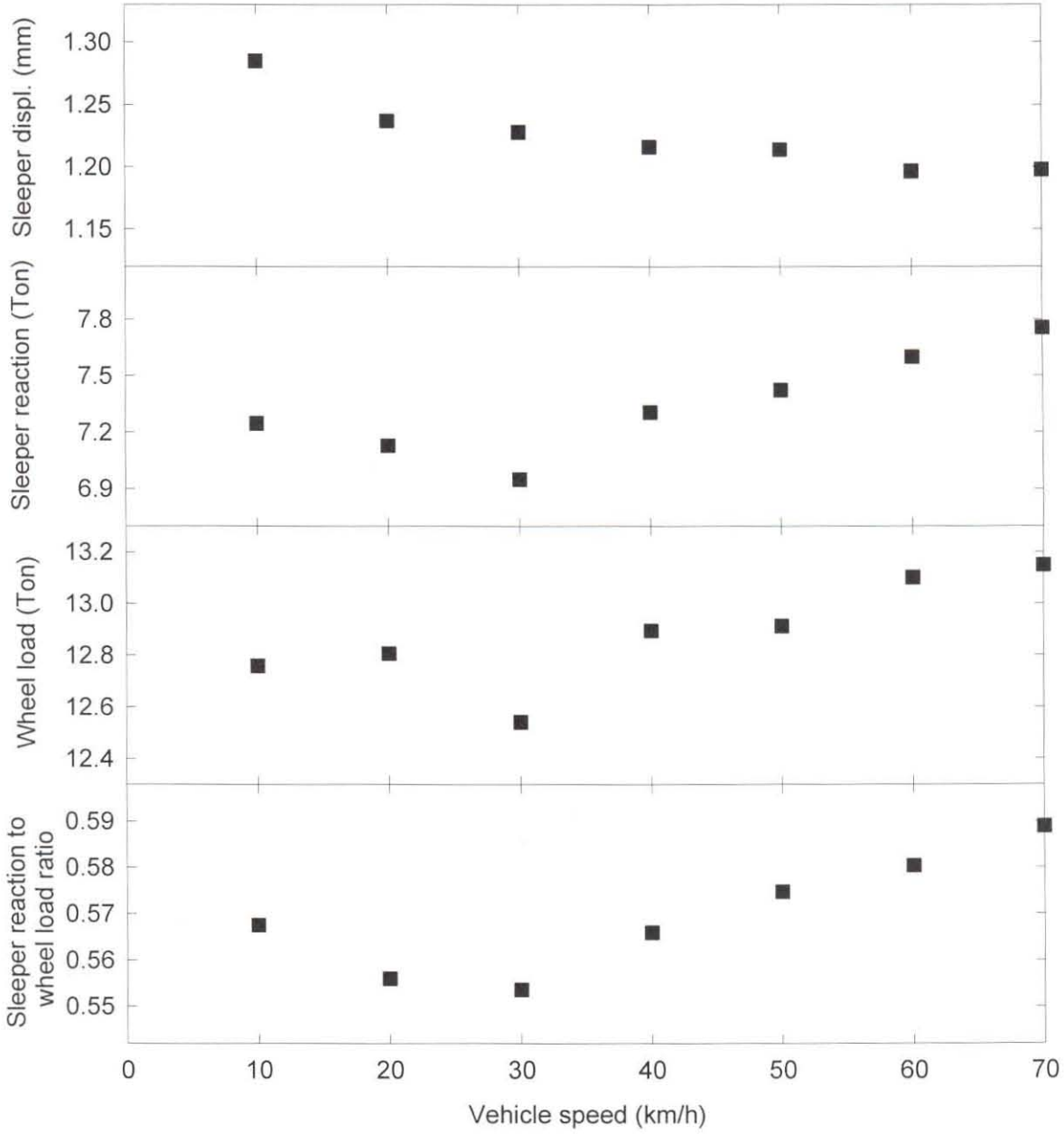

Figure B36: Dynamic track behaviour as a function of vehicle speed.

B.3.3 Vehicle and Track Performance Versus Accumulating Traffic

In this section the performance of the vehicle and the track is analysed as a function of accumulating traffic. Attention is given to the overall track settlement, the

development of track roughness, the changes in the dynamic wheel load, the behaviour of the vehicle suspension, the dynamic performance of the track, and changes in the sub-structure properties.

B.3.3.1 Track Settlement

Using digital levels, the absolute unloaded vertical space curve of the left and the right rail was measured over the 150 sleeper long test section. This was done directly after tamping and at regular intervals as the gross tonnage accumulated over the test site. As time went by, the time between measurements increased to adjust to the lower rate of track settlement. A curve of track settlement against million gross tons (MGT) of accumulating traffic is shown in Figure B37. From the figure it is clear that the rate of track settlement decreases as a function of accumulating cyclic track loading.

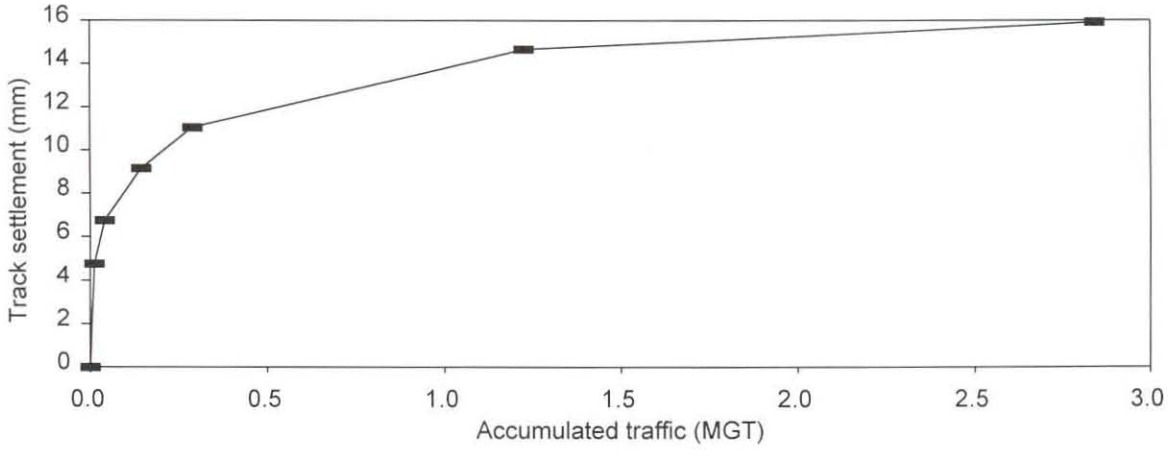

Figure B37: Average overall track settlement.

In Figure B38 the absolute vertical space curve as measured directly after tamping and after 2.84 MGT is shown together with a curve showing the relative differential track settlement.

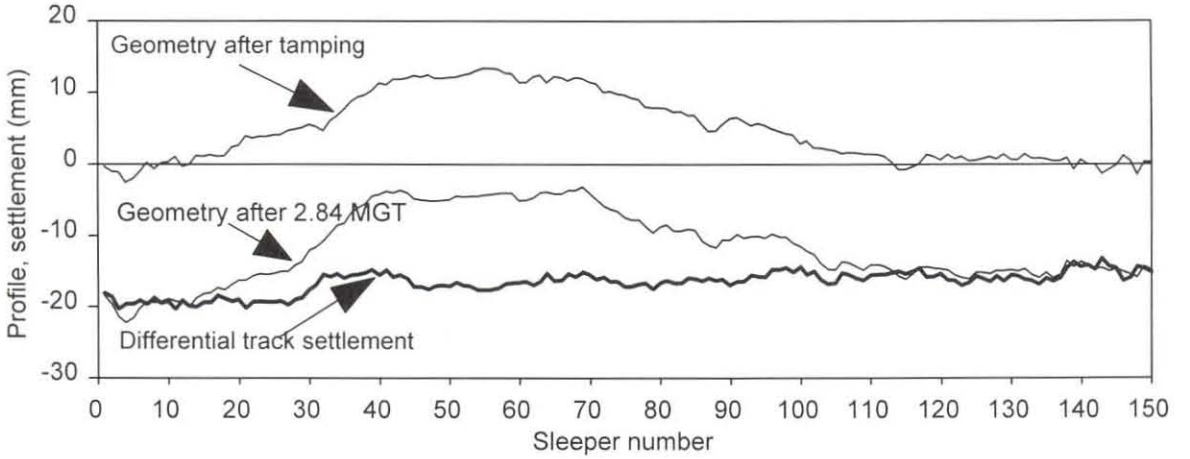

Figure B38: Track settlement profiles.

B.3.3.2 Track Roughness

Track roughness or track quality is directly related to differential track settlement and is defined as

$$R = \sqrt{\frac{\sum_{i=1}^{n} d_i^2}{n}} \qquad \text{(B6)}$$

where d_i = difference between the elevation of the point measured and the mean filtered elevation, and

n = number of measurements in the length of track under consideration.

The track roughness values that are plotted in Figure B39 represent a single roughness value calculated over the entire 150 sleeper section. As with the average track settlement, the increase in track roughness also decreases with accumulating traffic.

Track quality is the key to track load bearing capacity and efficient track maintenance. Generally track tamping is done to eliminate voids under the sleepers and to improve track quality before it becomes irreparable. This ensures safe

operation and good ride quality of passing vehicles. Although the concept of tamping is good something has to be done to make tamping effective over a longer time period. This can be achieved by for example spatial consolidation of the ballast layer after every tamping cycle. In contrast to natural settlement under train loading, the application of dynamic track stabilisation anticipates part of the initial settlement in a controlled way, without causing any change in the vertical track geometry. The subsequent further settlements are therefore smaller, the maintenance intervals become longer and the overall maintenance cost drops.

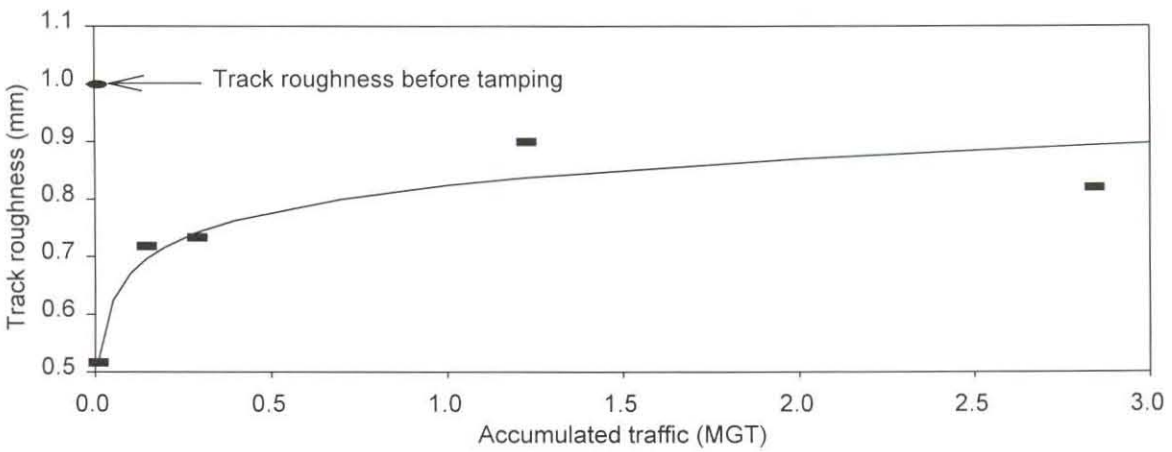

Figure B39: Changes in average track roughness.

B.3.3.3 Dynamic Wheel Load

As seen before, the dynamic wheel load changes with changing vehicle speed. Some changes are also observed as a function of changing track roughness. The variation of the RMS of the dynamic wheel load as measured by the load measuring wheelset increases with accumulating traffic due to an increasing track roughness. This is shown in Figure B40 for a vehicle speed of 40 km/h.

A time trace showing the dynamic wheel load as measured on the leading left wheel of the test bogie directly after tamping and after 2.84 MGT is presented in Figure

B41. From the traces it can be seen that the dynamic wheel load changed its pattern due to changes in the effective loaded track geometry.

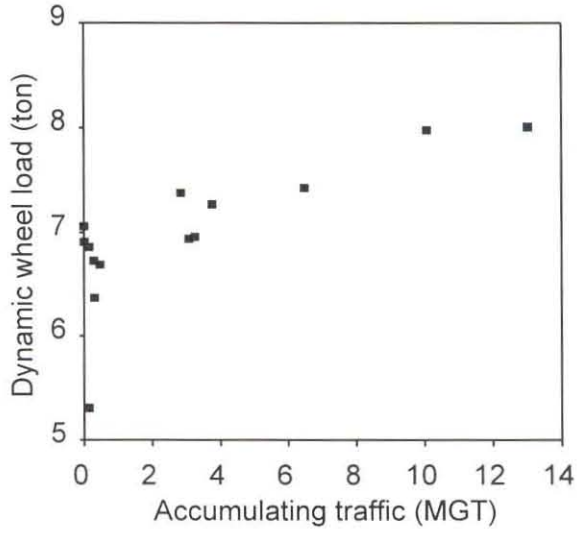

Figure B40: Variation of dynamic wheel load with accumulating traffic.

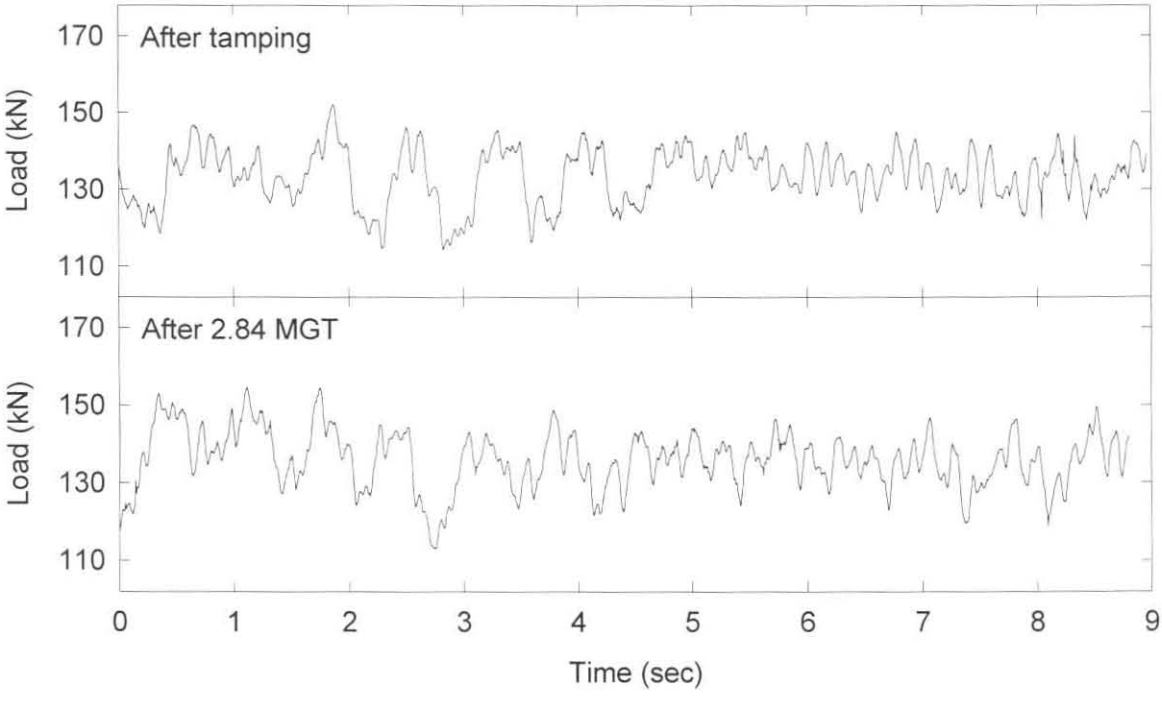

Figure B41: Wheel load as a function of accumulating traffic.

B.3.3.4 Vehicle Suspension Behaviour

A time trace showing the vertical displacement across the left side of the secondary suspension as measured directly after tamping and after 2.84 MGT is presented in Figure B42. From the traces it can be seen that the maximum displacement increased slightly, and that the overall displacement is still very small.

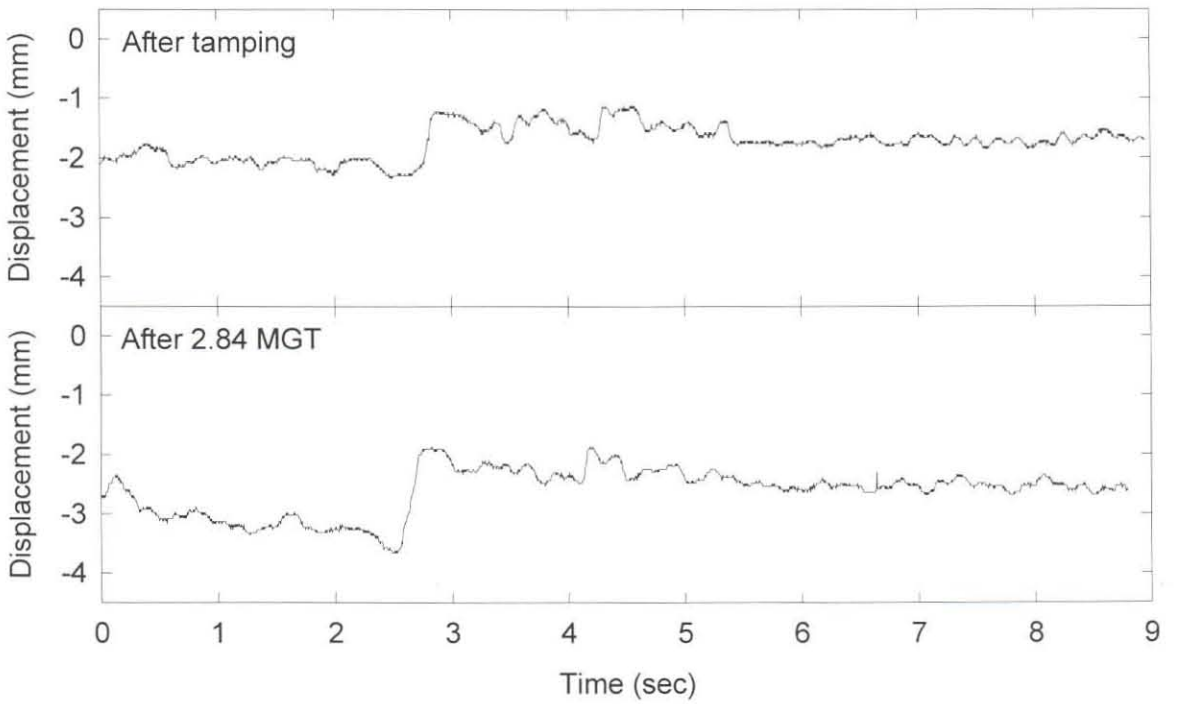

Figure B42: Displacement across secondary suspension as a function of accumulating traffic.

B.3.3.5 Dynamic Track Behaviour

The dynamic behaviour of the track as a function of accumulating traffic is discussed in terms of wheel load, sleeper reaction and sleeper deflection. In Figure B43, the behaviour as measured at Sleeper 73 and Sleeper 77 is given. Of particular importance in the interpretation of these two graphs is the fact that after 2.84 MGT a void was created at Sleeper 77. The resulting change in the dynamic behaviour

with respect to the sleeper reaction and the sleeper deflection of the track can clearly be seen.

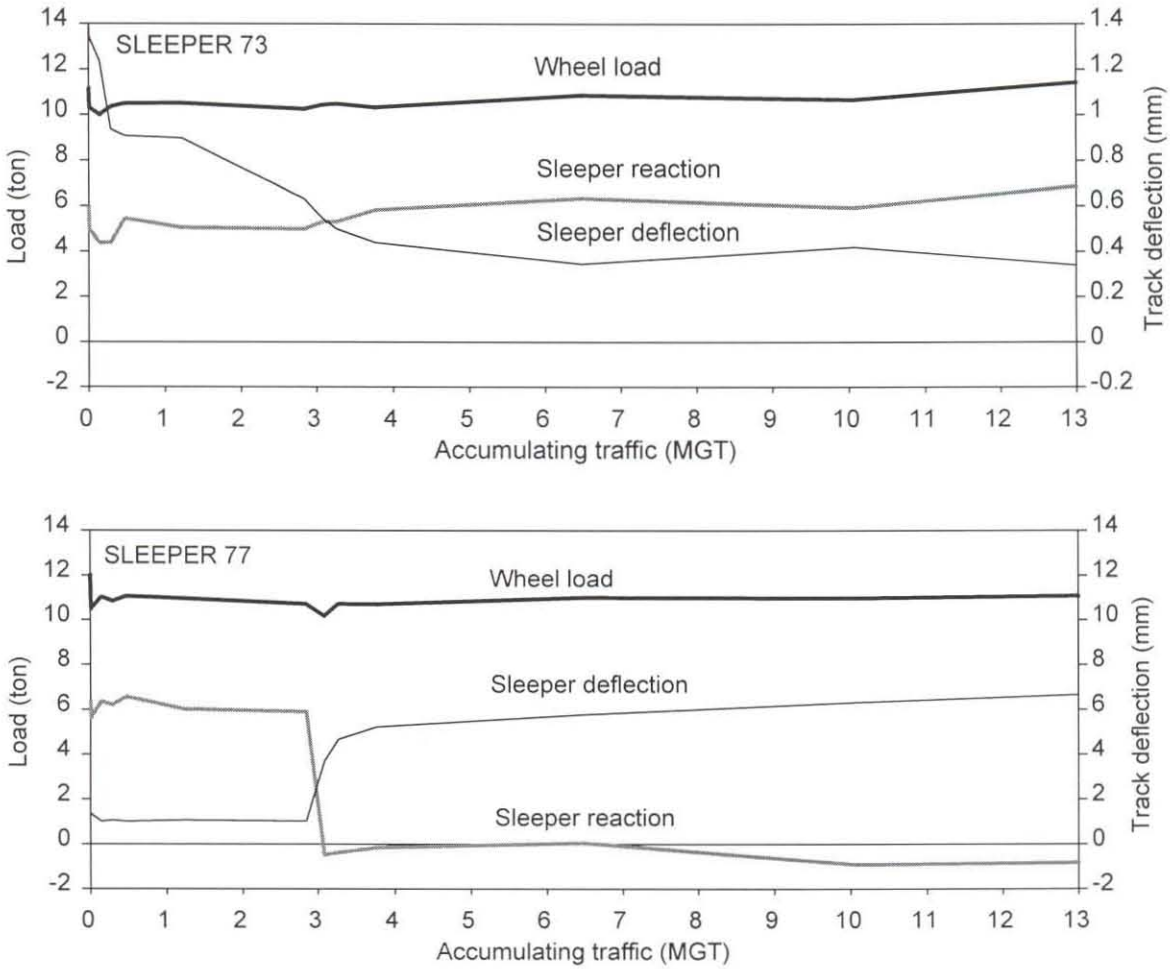

Figure B43: Wheel load, sleeper reaction and sleeper deflection at two different sleepers.

Every sleeper tends to have its own characteristic dynamic force deflection curve. There are variations with accumulating traffic, but in general a stiffer sleeper support stays stiffer, a softer sleeper support stays softer, a more nonlinear stiffness stays more nonlinear, and the hysteresis damping also does not change significantly. Variations in the dynamic track stiffness with accumulating tonnage are shown in Figure B44. Changes in the continuous plot of the static track deflection under a given load have already been shown in Figure B15.

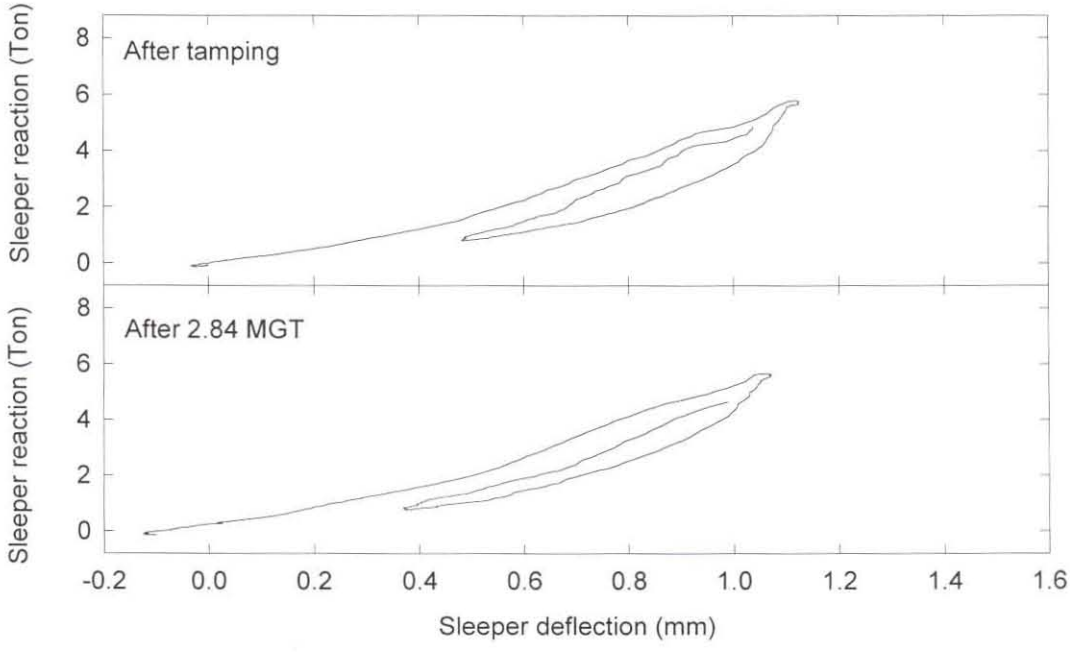

Sleeper 77

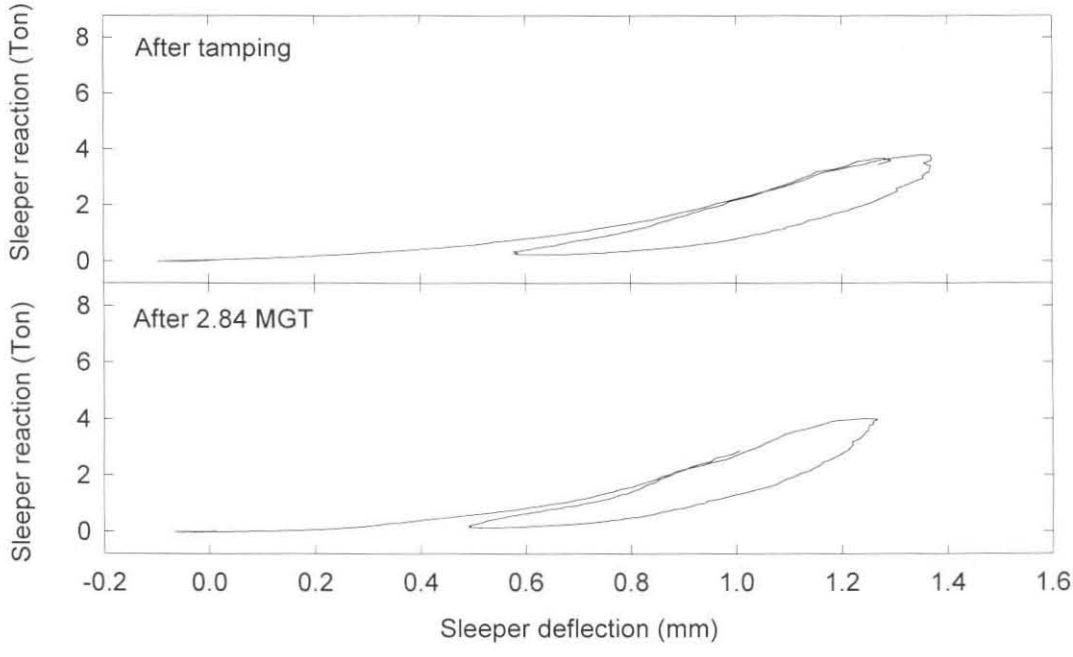

Sleeper 78

Figure B44: Changes in the dynamic track stiffness due to accumulating traffic.

B.3.3.6 Track Substructure Property

The property of the various substructure layers is best described in terms of their relevant modulus of elasticity, and the changes thereof as a function of accumulating traffic. The values of the various modulus of elasticity as given in Table B4 were derived from the MDD measurements using the technique described in Section B.2.4.1. The values were obtained for a 26 ton axle load. The modulus of elasticity as measured after 2.84 MGT shows a significant softening due to the excavation of a trench at the adjacent sleeper. The area of the trench was not tamped after being filled up to observe void forming.

Table B4: Modulus of elasticity of substructure layers.

Layer type	Ballast/ class	Sandy/ clay	Clay	Clay	Ballast/ class	Sandy/ clay	Clay	Clay
Layer depth	50-550mm	550-1050mm	1050-1250mm	1250-2550mm	50-550mm	550-1050mm	1050-1250mm	1250-2550mm
Tonnage MGT	Modulus of elasticity [Mpa] Left hand side				Modulus of elasticity [Mpa] Right hand side			
0.000	128	33	33	63	121	26	53	100
0.012	168	33	32	59	186	24	47	93
0.146	185	34	35	69	131	25	49	101
0.291	259	28	33	67	145	23	61	103
0.470	252	28	33	78	154	20	61	116
1.227	203	26	33	78	167	19	69	118
2.842	331	21	34	65	194	16	72	86
3.085	66	38	35	87	72	25	71	123
3.263	60	48	38	94	81	26	86	129

B.3.4 Void Forming

In Figure B43, it can be seen that the wheel load did not change significantly after the void was created. The sleeper reaction and sleeper displacement however showed a significant change because Sleeper 77 had lost its structural support and adjacent sleepers had to help carry the load. The result was an increased

differential ballast settlement in this area as can be seen in Figure B45. The resulting vertical displacement across the secondary suspension after 13 MGT is shown in Figure B46 together with the resulting wheel load. At this point in time there was still very little change in the dynamic behaviour of the test vehicle.

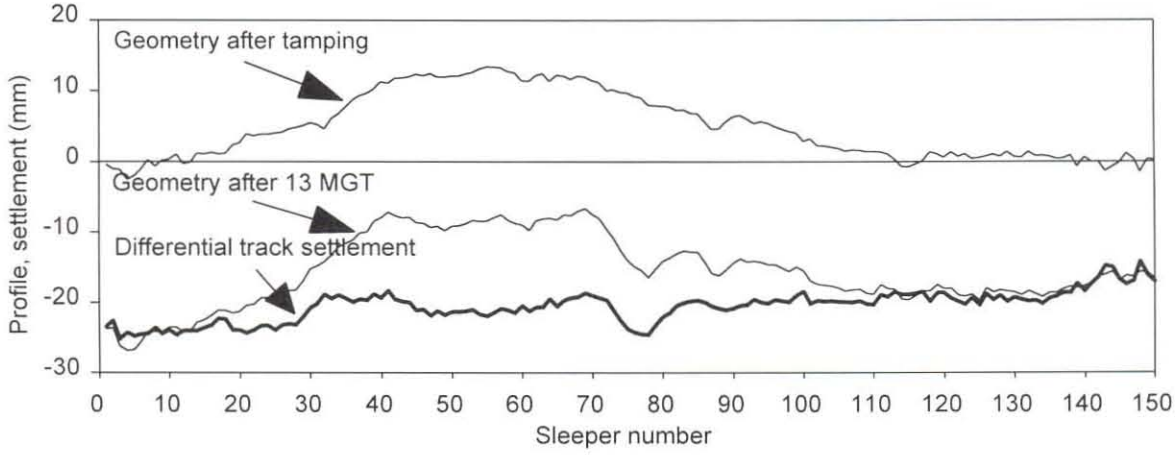

Figure B45: Differential ballast settlement after 13 MGT.

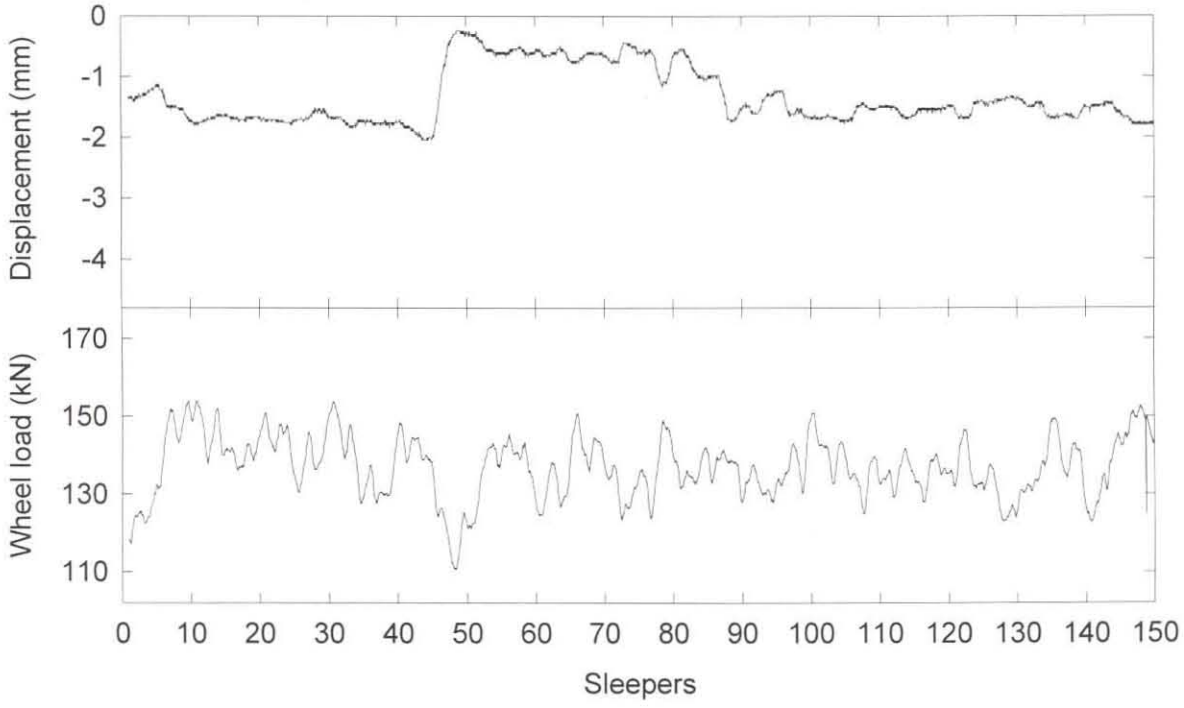

Figure B46: Dynamic vehicle behaviour including displacement across secondary suspension and dynamic wheel load.